PHYSICAL REVIEW E **95**, 031204(R) (2017)

X-ray shadow imprint of hydrodynamic instabilities on the surface of inertial confinement fusion capsules by the fuel fill tube

A. G. MacPhee,[1] D. T. Casey,[1] D. S. Clark,[1] S. Felker,[1] J. E. Field,[1] S. W. Haan,[1] B. A. Hammel,[1] J. Kroll,[1] O. L. Landen,[1] D. A. Martinez,[1] P. Michel,[1] J. Milovich,[1] A. Moore,[1] A. Nikroo,[1] N. Rice,[2] H. F. Robey,[1] V. A. Smalyuk,[1] M. Stadermann,[1] and C. R. Weber[1]

[1]*Lawrence Livermore National Laboratory, Livermore, California 94550, USA*

[2]*General Atomics, P.O. Box 85608, San Diego, California 92186-5608, USA*

(Received 14 October 2016; revised manuscript received 19 January 2017; published 30 March 2017; corrected 16 June 2017)

Measurements of hydrodynamic instability growth for a high-density carbon ablator for indirectly driven inertial confinement fusion implosions on the National Ignition Facility are reported. We observe significant unexpected features on the capsule surface created by shadows of the capsule fill tube, as illuminated by laser-irradiated x-ray spots on the hohlraum wall. These shadows increase the spatial size and shape of the fill tube perturbation in a way that can significantly degrade performance in layered implosions compared to previous expectations. The measurements were performed at a convergence ratio of ∼2 using in-flight x-ray radiography. The initial seed due to shadow imprint is estimated to be equivalent to ∼50–100 nm of solid ablator material. This discovery has prompted the need for a mitigation strategy for future inertial confinement fusion designs as proposed here.

DOI: 10.1103/PhysRevE.95.031204

Hydrodynamic instabilities are a major concern for inertial confinement fusion (ICF) implosions [1–4] and considerable effort has been invested to characterize and mitigate against them [5–24]. For indirect-drive implosions at the National Ignition Facility (NIF) [25–27], a cryogenic deuterium-tritium (DT) fuel layer is imploded by ablative acceleration of an outer shell driven by x rays generated in an enclosing hohlraum. The hohlraum is irradiated with up to 1.9 MJ laser energy at up to 500 TW peak power, accelerating the shell to ∼400 km/s to achieve the ∼3000× solid DT fuel density required for ignition. Outer surface capsule imperfections can evolve during shock transit through the shell due to the ablative Richtmyer-Meshkov instability [28–32] followed by further amplification during the acceleration phase of the implosion by the Rayleigh-Taylor (RT) instability [33]. These modulations can feed through the shell to the DT ice layer and seed a subsequent phase of RT growth during the deceleration phase of the implosion toward peak compression. These imperfections can lead to a distorted, asymmetric hot spot, significantly limiting the temperature, pressure, and neutron yield attainable. In extreme cases ablator material can penetrate through the shell into the hot spot to mix with the DT fuel prior to peak compression, reducing temperature further by radiative cooling and resulting in even more dramatic performance and yield degradation [34–37].

It has been clear for some time that the support tent contribution to capsule hydrodynamic instability growth [13,38,39] is very important, while it has been thought that the fill tube perturbation was less significant. Recent layered DT implosions with high-density carbon (HDC) ablators [40] unexpectedly observed a dramatic feature in x-ray images near stagnation coming from the direction of the fill tube. The yield over calculated yield for these implosions was ∼30%, despite the low compression relative to typical high-performance NIF implosions. The work discussed here indicates the possibility that a significant degradation even at low convergence could be due to the fill tube perturbation. Previous experiments on the Z facility [41] prior to the National Ignition Campaign (NIC [26,42]) measured the hydrodynamic growth of the fill tube perturbation using side-on x-ray radiography. These measurements agreed with 2D Hydra simulations and this code was subsequently used to model the fill tube effect for the NIC experiments. This predicted an acceptable contribution to the performance degradation in layered DT implosions. In this Rapid Communication, we present measurements of hydrodynamic instability growth for a high-density carbon ablator for ICF on the NIF. These include measurements of the fill tube perturbation measured with face-on x-ray radiography. We discovered that the fill tube perturbation is in fact considerably larger and more complicated than expected, due to three-dimensional (3D) effects not captured in the previous study. We infer that x-ray spots where the hohlraum wall is laser illuminated early in the laser drive, cast x-ray shadows of the glass fill tube onto the capsule surface. This imprints an azimuthal hydrodynamic instability about the fill tube due to modulation of the ablation rate as a function of angle around the fill tube. These shadows increase the spatial size of the expected fill tube perturbation to the extent that the feature can grow and break through the shell at low convergence and therefore significantly degrade performance in layered implosions compared to previous expectations. This discovery has prompted the need for a mitigation strategy for future ICF designs for which we suggest one promising method below.

Following previous studies of instability growth for both native surface roughness and preimposed modulations [6,8,10], we have performed x-ray radiographic measurements to characterize the instability growth in HDC, including the fill tube. The experimental platform for hydrogrowth radiography is illustrated in Fig. 1 and described in detail in [4]. The hohlraum wall material was uranium, 10.13 mm long by 5.74 mm diameter with 3.38 mm diameter laser entrance holes (LEHs). The azimuthal and polar radii of the inner 30° and outer 44.5° spots were (0.82 × 1.18) mm and (0.64 × 0.52) mm, respectively. The capsule ablator was 3.5 g/cc polycrystalline diamond (HDC [43]) with outer radius $r_0 = 908\,\mu$m and

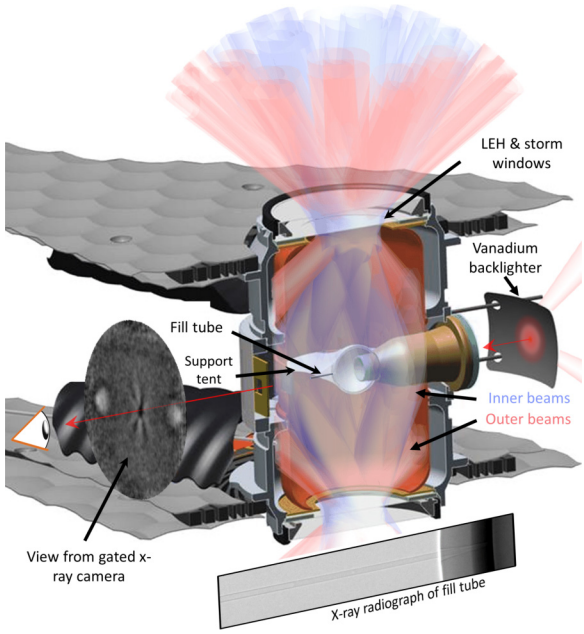

FIG. 1. Experimental platform. Outer (red) and inner (blue) laser quads; two outer quads above and below the fill tube are repurposed to excite the x-ray backlighter. Inset: x-ray radiograph of fill tube.

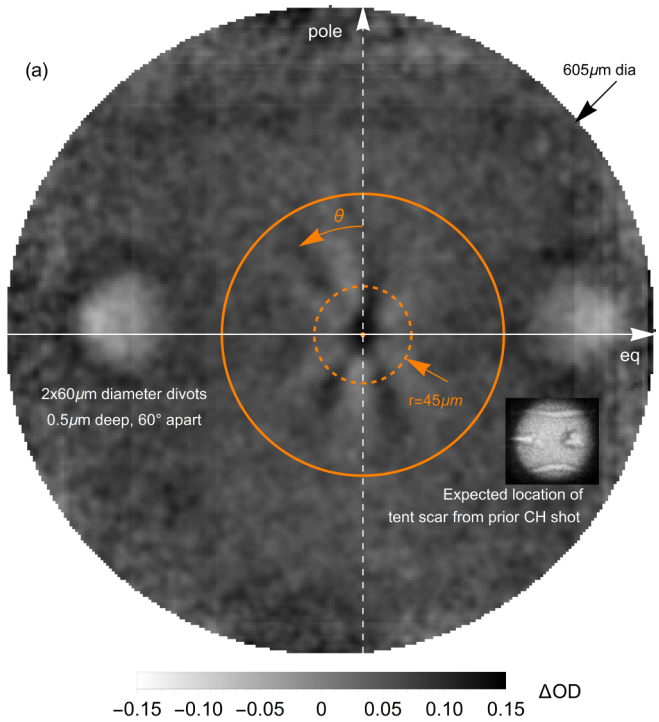

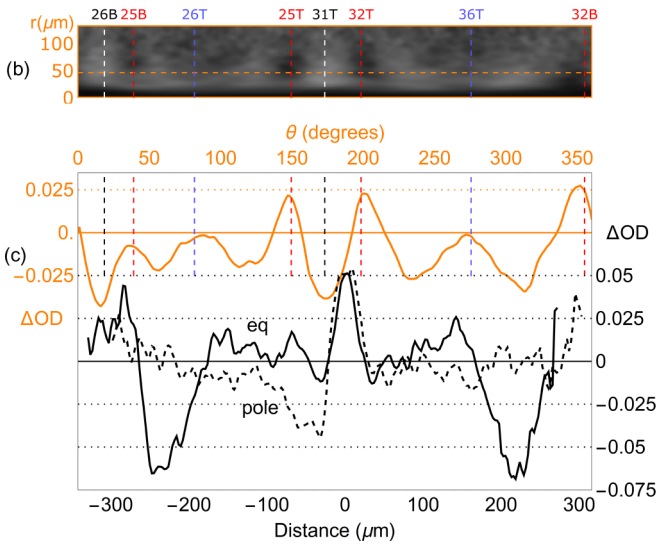

FIG. 2. Optical density modulation in (a) spatial coordinates, (b) r,θ coordinates, (c) lineouts along the equator, pole, and θ at $r = 45\ \mu$m. Inset: Radiograph for a CH capsule showing expected tent location. The dashed lines in (b) correspond to the ray-traced orientation of the fill tube shadows.

thickness 64 μm. The inner 25 μm of the ablator was doped with 0.25 at. % tungsten, which for a layered fuel capsule acts as a preheat shield to control the ablator density profile near the DT fuel (for a detailed discussion on target surrogacy, see [44]). The fill tube, shown in the radiograph inset at the bottom of Fig. 1, was 1 mm-long borosilicate glass with density 2.33 g/cc, outer radius 5 μm, and inner radius 2.5 μm. The fill tube was attached to the capsule using glue in a conical hole drilled into the capsule wall. Time-gated radiographs of the capsule transmission were recorded along the fill tube axis at a convergence ratio r_0/r of 2.1 ± 0.1 using an array of thirty 16-μm-diameter imaging pinholes and an 80-ps duration gate. The source to pinhole distance was 80 mm and the magnification onto the gated microchannel plate was 7.8×. The effective x-ray backlighter energy was ~6.8 keV, comprising vanadium He-α and higher-energy continuum emission from a vanadium foil irradiated at 10^{15} W cm^{-2}.

Figure 2(a) is the x-ray radiograph of the implosion in units of optical depth modulation (ΔOD) averaged over all 30 discrete pinhole images. Here $\Delta\text{OD} = -\Delta\ln(I/I_0) = \Delta\int\kappa\rho dR$ where κ is the opacity at the x-ray backlighter energy and ρdR is the projected areal density. I and I_0 are the transmitted and incident backlighter intensities, respectively. The horizontal axis is parallel to the equatorial plane through two reference divots laser-machined into the outer surface of the capsule, 60-μm-diameter, 0.5-μm-deep, and separated 60° about the fill tube axis. The reduction in separation of these features at the time of the radiograph corresponds to the capsule convergence of ~2. The vertical axis is parallel to the hohlraum axis and passes through the center of the upper (30 nm) and lower (45 nm) Formvar capsule support tents. Figure 2(b) is the portion of the radiograph within the outer (solid) circle from Fig. 2(a) plotted as a function of radius r and angle θ about the fill tube using the same ΔOD grayscale. The dashed vertical lines in Figs. 2(b) and 2(c) are the calculated angle of the fill tube shadows for the corresponding laser beams from ray tracing. Lineouts through the divots (solid), the equator and tents (dashed), and an azimuthal lineout about the fill tube at radius $r = 45\ \mu$m (orange, upper) are shown in Fig. 2(c).

Two striking features are apparent: (i) No modulation was observed due to the tent using the HDC ablator. This is significant relative to the tent perturbations that were observed in previous measurements with CH ablators [13]

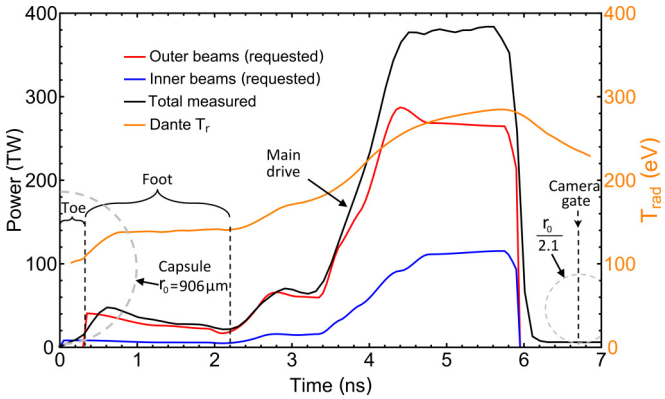

FIG. 3. Laser pulse shape for the inner and outer quads. Hohlraum T_r (Dante) reaches ~100 eV during the toe and rises to 140 eV in the foot. Insets at time 0 at 6.7 ns show the relative capsule radii, initially and at the time of the backlit image.

at similar convergence. A tent modulation for HDC ablators has been observed in self-emission measurements later in time, suggesting the dynamics of this perturbation growth is different from CH ablators. The expected location of the tent modulation is illustrated by the dashed white curves in Fig. 2(a), based on the position of the tent modulation observed for a previous shot using a plastic ablator where the growth is significantly greater, as shown in the inset [13,38,45]. (ii) An unexpected pattern of radial "spoke" modulations was observed, centered on the fill tube modulation. The instability due to both the radial spoke pattern and the fill tube itself exhibit similar peak-to-peak optical density (OD) modulation ~0.05 shown in the lineouts in Fig. 2(c). The structure of the radial OD modulation pattern can be correlated with the orientation of beam spots. As described in more detail below, we infer that the features are due to imprint of an azimuthal instability on the capsule surface due to modulation of the ablation rate around the fill tube early in the laser drive. The seed of the modulation is produced by x-ray radiation from spots on the hohlraum wall corresponding to outer laser beams that have a view of the capsule surface obstructed by the fill tube, causing a pattern of shadows about the fill tube in which ablation of the capsule surface is reduced. The laser pulse shape, hohlraum geometry, beam pointing, and gas fill for ICF implosions on the NIF have been designed to deliver a uniform spherical capsule implosion using indirect cylindrical x-ray drive. As indicated in the beam layout in Fig. 1 and the laser pulse shape in Fig. 3, the relatively low-intensity inner beams switch on first (the "toe" of the laser pulse), blowing down the LEH windows at either end of the hohlraum, followed ~300 ps later by the more intense outer beams. (The curve for "Total measured" power in Fig. 3 is broadened by instrument response and does not faithfully represent the details of the toe. Those details are best envisioned using the individual requested pulses, with the actual rise broadened by ~150 ps for the inner cone and ~200 ps for the outer cone.) The delay between the cones allows the plasma density in the window to drop below quarter-critical density and avoid significant subsequent hot-electron production by the outer beams due to two-plasmon decay [46,47]. (Hot electrons can be a significant contribution to preheat of the deuterium-tritium fuel ice layer in the capsule, which can prevent the target reaching compression suitable for ignition.) During the "toe," the laser intensity on the uranium hohlraum wall is $\sim 3 \times 10^{13}$ W cm^2, while the intensity of outer cone spots during the foot is $\sim 1.3 \times 10^{14}$ W cm^2. The foot generates sufficient soft x rays to drive the capsule with a hohlraum radiation temperature reaching T_r of ~140 eV in 0.7 ns.

The glass fill tube is initially opaque to this <keV Planckian x-ray radiation and can be expected to cast an x-ray shadow on the surface of the capsule near its base until ablation, ionization, and expansion have reduced the fill tube shadowing. With an average expansion velocity of the order of the sound speed $\sqrt{(ZT_e/m_i)} \sim 70\,\mu$m/ns (assuming $T_e \approx 0.8T_r$ and $Z/A \approx$ ½ and average $T_r = 120$ eV over the first 0.7 ns from the Dante measurement in Fig. 3) and mass ablation rate for the borosilicate fill tube ≈3 μm/ns (scaling from ablation rate measurements for CH [18,48]), we expect the tube shadowing to become negligible about ~0.5–0.7 ns after the start of the drive. By this time the L shell of oxygen and the L and M shell electrons of silicon comprising the ablated fill tube material will be stripped and the areal density reduced >10×.

During this first 0.5 ns, the capsule illumination is dominated by the outer beam spots as estimated by the following argument: The ratio of hohlraum wall x-ray reradiation to laser-produced x rays is given by $\alpha/(1-\alpha)$ where α is the hohlraum albedo defined as the ratio of reemitted flux to incident flux. The uranium hohlraum albedo can be estimated to rise as $1 - 0.4/T_r{}^{0.7}t^{0.4}$ with T_r in heV (100 eV units [2]), t in nanoseconds with respect to the start of the foot, and the 0.4 constant is set by a measured α~0.65 at 1.5 ns for $T_r = 100$ eV [49]. Hence, 0.3 ns after the start of the foot (or 0.6 ns after the start of the toe), α has only reached 0.5 and the wall power has just become comparable to the spot power. The laser-produced x-ray flux reaching the capsule waist can be assumed to be dominated at those times by the outer beam spots as despite being 1.5× further from the capsule, they have 4× more power than the inner beam spots as shown in Fig. 3.

To confirm this correspondence, we performed 3D geometric ray tracing of the hohlraum/capsule/fill tube system from source spots on the hohlraum wall; specifically, those with a view of the capsule obstructed by the fill tube and which could therefore form a shadow of the fill tube on the capsule surface. Eight laser spots, four from each end (each about 1 mm in azimuthal extent, filling the azimuth with minimal overlap), dominate the illumination at the base of the fill tube (at ≈±45° in azimuth to the fill tube). Of those, two quads (four beams in each of Q31T and Q26B) were used to drive the backlighter and their absence adds to the complexity of the spoke pattern. For a 1mm diameter outer beam spot ~3 mm away from the fill tube base viewed at an angle of ~45° to its axis, a 10 μm diameter tube would cast an umbra to about 10 μm × sin 45° × (3 mm/1 mm) = 20 μm from the fill tube base, as seen in the inset in Fig. 4. The fact that the imprint extends about 200 μm from the base (in the initial unconverged frame of reference) suggests shadow imprint is still occurring when the fill tube diameter has expanded 10× to 100 μm, consistent with the earlier estimate of minimum tube expansion to go transparent and the transverse spatial scale of the shadows. The axes of the shadows cast by each spot are shown in Figs. 2(b) and 4 overlaid on the radiograph.

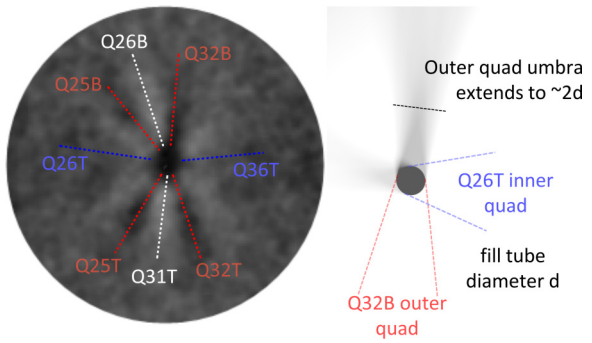

FIG. 4. Left: Fill tube shadow orientation (dashed lines) for the outer quads (red), lower intensity inner quads (blue), and missing backlighter quads (white). Right: Shadow cast by inner (Q26T) and outer (Q32B) laser spots. The length of the umbra for the outer quads scales as ~2× the fill tube diameter, suggesting a 100-μm effective shadowing diameter for the expanded tube, prior to the capsule convergence by ~2.

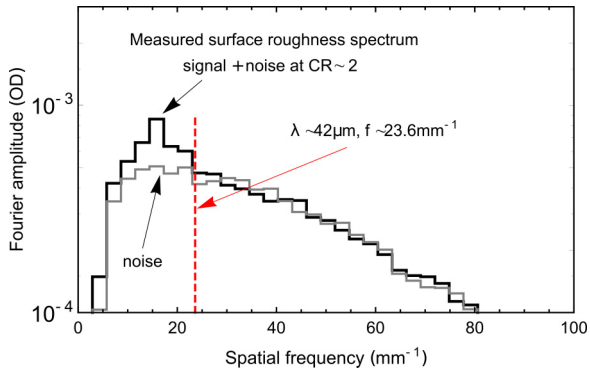

FIG. 5. Surface roughness and noise for HDC capsule at CR ~2. There is no evidence of native roughness seeds with suitable frequency and amplitude to generate the spoke feature.

The ray tracing was performed with the capsule at its initial diameter and included a fill tube tilt of ~2.5° clockwise and 2.1° down as obtained from target metrology. The dashed lines representing the shadow orientation in both figures align with the regions in the data with greatest optical depth, indicating regions with reduced ablation early in the drive. The orientation of the missing shadows that would have been cast by the two missing quads that drove the backlighter is shown in white. These regions exhibit reduced optical depth bubbles, as a consequence of the growth of the adjacent high-density spikes associated with the corresponding outer quad shadows. Bubbles also appear on the outer edges of the high-density spikes because of Rayleigh-Taylor flow into the spikes.

The measured peak to valley $\Delta\mathrm{OD} = 0.05$ (0.09 with modulation transfer function correction) is the same column density as 32 μm of C at initial density. To evaluate the corresponding perturbation growth, we can estimate the magnitude of the initial perturbation seed formed on the surface of the capsule by calculating the difference in ablation rate between the area in the umbra of the fill tube (where there is illumination by three outer quads) and the area exposed to all four outer quads. At an average $T_r = 120$ eV during the first 0.3 ns of foot drive, the mass ablation rate for the diamond ablator $\approx T_r{}^3$ is 2.0 μm/ns in the preshocked reference frame [18,48]. So, the differential mass ablated should be $1/4 \times 2.0\,\mu\mathrm{m/ns} \times 0.3$ ns ≈ 150 nm. (The differential ablation could be as small as 50 nm, depending on the time-averaged shadow dilution due to the wall and inner beam emission.) This implies an optical density growth factor of ≈200–300. The transverse scale length corresponds to a mode number of about 64 (λ~42 μm). This is slightly larger than the simulated growth of initial topographic perturbations, for which the peak optical density growth factor is ~200. The larger growth from illumination variations could result from a velocity amplitude in the initially seeded modulation.

For the case of implosions with no outer beams removed for radiography, the shadow imprint pattern would be different. Specifically, there would be a gradual increase in ablation rate as one moves past ≈±45° from the fill tube azimuth, creating a cross pattern of spikes on the inside and bubbles on the outside, with growth similar to that measured here. With the shadow imprint extending ~200 μm from the tube axis, the shadow imprinted perturbation subtends a ~22° conical hole in the side of the implosion, which at peak compression would be expected to have a significant impact on capsule performance. These shadows serve as important seeds to perturbation growth: modes with high growth, around mode 60, are seeded by the individual beams' shadows, while the global structure subtends substantial solid angle and makes for a large final perturbed volume.

By comparison, experiments also have been done with the same overall configuration but no fill tube. No structure is evident around the center point of the image. Figure 5 illustrates the OD amplitude versus spatial frequency of this case, measured at the same convergence. The OD amplitude spectrum (bold curve) including noise (light curve) is the average radial profile of the absolute value of the two-dimensional (2D) fast Fourier transform over a 360 × 360 μm region in the center of the x-ray image averaged over 14 pinholes. The noise is derived from the difference spectrum between the two sets of adjacent images. Some perturbation growth is evident above the noise, mostly at modes around 15 mm^{-1} (spherical harmonic mode ~40). Very little amplitude is evident at mode 64, corresponding to 23.6 mm^{-1}. The observed modulations are probably from surface roughness, but detailed analysis of this control experiment is beyond the scope of this Rapid Communication. This experiment does demonstrate that the features seen in the center of Fig. 2(a) are not a result of the intrinsic surface roughness of the capsule.

The significance of this new effect depends on details of the ICF pulse shape design. A long toe (up to 1.2 ns, as used in the three-shock high-foot [50] and adiabat-shaped designs [51]) should reduce seeding as the fill tube blows down more before the outer beams turn on. A lower foot T_r should lead to less differential mass ablation and less seeding; for example, the 70-eV four-shock low foot CH design [4] should have 2× reduced seeding compared to the current 120-eV HDC design. Note that the fill tube expansion $\sim\sqrt{T_e t}$ scales as $1/T_r{}^{1.25}$ for a given level of shadow dilution, so increases for lower T_r, but

that is offset by a higher fill tube opacity when averaged over a lower T_r drive spectrum.

In conclusion, we have observed a larger than expected modulation pattern imprinted on the surface of an ICF implosion capsule consistent with differential ablation induced by shadowing by the fill tube of x-ray emission from discrete laser spots on the wall of the hohlraum. From the equivalent experiment without a fill tube there is no evidence of a suitable native capsule seed capable of producing the observed effect. The optical depth peak-to-valley modulation normalized to the total optical depth of the shell at measured convergence is ∼30%. The shadow imprint grows at mode ∼60, near the peak of the growth factor dispersion curve. This fill tube perturbation is expected to grow significantly during subsequent evolution toward peak velocity. This is consistent with large perturbations that dominated the x-ray image for the corresponding layered DT implosions [40]. A fill tube mitigation campaign is now under way and is recognized as a high priority for the national indirect-drive ICF program.

The full impact of the azimuthal instability cannot be inferred from 2D simulations and we are working toward a predictive model for the impact of shadow imprint on yield using more detailed 3D simulations. For future ICF implosions we propose a mitigation strategy using an extended toe to provide more time for the fill tube to blow down prior to applying the outer cone drive beams that dominate the shadow imprint mechanism. 2D hohlraum simulations are under way to optimize this drive.

This work was performed under the auspices of the U.S. Department of Energy by Lawrence Livermore National Laboratory under Contract No. DE-AC52-07NA27344.

[1] J. H. Nuckolls, L. Wood, A. Thiessen, and G. Zimmerman, Nature (London) **239**, 139 (1972).
[2] J. D. Lindl, P. Amendt, R. L. Berger *et al.*, Phys. Plasmas **11**, 339 (2004).
[3] J. H. Nuckolls, J. Phys.: Conf. Ser. **244**, 012007 (2010).
[4] S. W. Haan, J. D. Lindl, D. A. Callahan *et al.*, Phys. Plasmas **18**, 051001 (2011).
[5] V. A. Smalyuk, D. T. Casey, D. S. Clark, M. J. Edwards, S. W. Haan, A. Hamza, D. E. Hoover, W. W. Hsing, O. Hurricane, J. D. Kilkenny, J. Kroll, O. L. Landen, A. Moore, A. Nikroo, L. Peterson, K. Raman, B. A. Remington, H. F. Robey, S. V. Weber, and K. Widmann, Phys. Rev. Lett. **112**, 185003 (2014).
[6] K. S. Raman, V. A. Smalyuk, D. T. Casey *et al.*, Phys. Plasmas **21**, 072710 (2014).
[7] D. T. Casey, V. A. Smalyuk, K. S. Raman *et al.*, Phys. Rev. E **90**, 011102(R) (2014).
[8] V. A. Smalyuk, M. Barrios, J. A. Caggiano *et al.*, Phys. Plasmas **21**, 056301 (2014).
[9] V. A. Smalyuk, S. V. Weber, D. T. Casey *et al.*, Phys. Plasmas **22**, 080703 (2015).
[10] A. G. MacPhee, J. L. Peterson, D. T. Casey *et al.*, Phys. Plasmas **22**, 080702 (2015).
[11] V. A. Smalyuk, S. V. Weber, D. T. Casey *et al.*, High Power Laser Sci. Eng. **3**, e17 (2015).
[12] S. W. Haan, H. Huang, M. A. Johnson *et al.*, Phys. Plasmas **22**, 032708 (2015).
[13] V. A. Smalyuk, S. V. Weber, D. T. Casey *et al.*, Phys. Plasmas **22**, 072704 (2015).
[14] D. S. Clark, C. R. Weber, J. L. Milovich *et al.*, Phys. Plasmas **23**, 056302 (2016).
[15] J. L. Peterson, D. T. Casey, O. A. Hurricane *et al.*, Phys. Plasmas **22**, 056309 (2015).
[16] D. T. Casey *et al.*, Phys. Rev. Lett. **115**, 105001 (2015).
[17] D. S. Clark, C. R. Weber, V. A. Smalyuk *et al.*, Phys. Plasmas **23**, 072707 (2016).
[18] O. L. Landen, K. L. Baker, D. S. Clark *et al.*, J. Phys.: Conf. Ser. **717**, 012034 (2016).
[19] H. F. Robey, V. A. Smalyuk, J. L. Milovich *et al.*, Phys. Plasmas **23**, 056303 (2016).
[20] V. N. Goncharov, J. P. Knauer, P. W. McKenty *et al.*, Phys. Plasmas **10**, 1906 (2003).
[21] G. Fiksel, S. X. Hu, V. A. Goncharov *et al.*, Phys. Plasmas **19**, 062704 (2012).
[22] S. X. Hu, G. Fiksel, V. N. Goncharov, S. Skupsky, D. D. Meyerhofer, and V. A. Smalyuk, Phys. Rev. Lett. **108**, 195003 (2012).
[23] M. Karasik, J. L. Weaver, Y. Aglitskiy, J. Oh, and S. P. Obenschain, Phys. Rev. Lett. **114**, 085001 (2015).
[24] C. R. Weber, T. Döppner, D. T. Casey, T. L. Bunn, L. C. Carlson, R. J. Dylla-Spears, B. J. Kozioziemski, A. G. MacPhee, A. Nikroo, H. F. Robey, J. D. Sater, and V. A. Smalyuk, Phys. Rev. Lett. **117**, 075002 (2016).
[25] E. I. Moses, R. N. Boyd, B. A. Remington *et al.*, Phys. Plasmas **16**, 041006 (2009); G. H. Miller, E. I. Moses, and C. R. Wuest, Opt. Eng. **443**, 2841 (2004).
[26] N. B. Meezan, M. J. Edwards, O. A. Hurricane *et al.*, Plasma Phys. Control. Fusion **59**, 014021 (2017).
[27] V. A. Smalyuk *et al.*, Phys. Rev. Lett. **111**, 215001 (2013).
[28] V. N. Goncharov, Phys. Rev. Lett. **82**, 2091 (1999).
[29] Y. Aglitskiy, A. L. Velikovich, M. Karasik, V. Serlin, C. J. Pawley, A. J. Schmitt, S. P. Obenschain, A. N. Mostovych, J. H. Gardner, and N. Metzler, Phys. Rev. Lett. **87**, 265001 (2001).
[30] E. E. Meshkov, Izv. Acad. Sci. USSR Fluid Dyn. **4**, 101 (1969); R. D. Richtmyer, Commun. Pure Appl. Math. **13**, 297 (1960).
[31] E. N. Loomis, D. Braun, S. H. Batha *et al.*, Phys. Plasmas **18**, 092702 (2011).
[32] E. Loomis, D. Braun, S. H. Batha, and O. L. Landen, Phys. Plasmas **19**, 122703 (2012).
[33] Lord Rayleigh, Proc. London Math. Soc. **s1-14**, 170 (1882); G. I. Taylor, Proc. R. Soc. London, Ser. A **201**, 192 (1950).
[34] M. J. Edwards, J. D. Lindl, B. K. Spears *et al.*, Phys. Plasmas **18**, 051003 (2011).
[35] S. P. Regan *et al.*, Phys. Rev. Lett. **111**, 045001 (2013).
[36] T. Ma *et al.*, Phys. Rev. Lett. **111**, 085004 (2013).
[37] C. R. Weber, D. S. Clark, A. W. Cook *et al.*, Phys. Plasmas **22**, 032702 (2015).
[38] R. Tommasini, J. E. Field, B. A. Hammel *et al.*, Phys. Plasmas **22**, 056315 (2015).

[39] S. R. Nagel, S. W. Haan, J. R. Rygg *et al.*, Phys. Plasmas **22**, 022704 (2015).

[40] L. Divol, Progress towards a one-dimensional layered DT implosion using HDC capsules at the NIF, Bull. Am. Phys. Soc. **61**, UI3.00001 (2016).

[41] G. R. Bennett *et al.*, Phys. Rev. Lett. **99**, 205003 (2007).

[42] J. Lindl, O. Landen, J. Edwards *et al.*, Phys. Plasmas **21**, 020501 (2014).

[43] S. Le Pape, L. F. Berzak Hopkins, L. Divol *et al.*, Phys. Plasmas **23**, 056311 (2016).

[44] O. L. Landen, J. Edwards, S. W. Haan *et al.*, Phys. Plasmas **18**, 051002 (2011).

[45] J. L. Milovich, H. F. Robey, D. S. Clark *et al.*, Phys. Plasmas **22**, 122702 (2015).

[46] P. Michel, L. Divol, E. L. Dewald, J. L. Milovich, M. Hohenberger, O. S. Jones, L. Berzak Hopkins, R. L. Berger, W. L. Kruer, and J. D. Moody, Phys. Rev. Lett. **115**, 055003 (2015).

[47] E. L. Dewald, F. Hartemann, P. Michel, J. Milovich, M. Hohenberger, A. Pak, O. L. Landen, L. Divol, H. F. Robey, O. A. Hurricane, T. Döppner, F. Albert, B. Bachmann, N. B. Meezan, A. J. MacKinnon, D. Callahan, and M. J. Edwards, Phys. Rev. Lett. **116**, 075003 (2016).

[48] R. E. Olson, G. A. Rochau, O. L. Landen, and R. J. Leeper, Phys. Plasmas **18**, 032706 (2011).

[49] O. S. Jones, S. H. Glenzer, L. J. Suter, R. E. Turner, K. M. Campbell, E. L. Dewald, B. A. Hammel, J. H. Hammer, R. L. Kauffman, O. L. Landen, M. D. Rosen, R. J. Wallace, and F. A. Weber, Phys. Rev. Lett. **93**, 065002 (2004).

[50] T. R. Dittrich, O. A. Hurricane, D. A. Callahan, E. L. Dewald, T. Döppner, D. E. Hinkel, L. F. Berzak Hopkins, S. Le Pape, T. Ma, J. L. Milovich, J. C. Moreno, P. K. Patel, H.-S. Park, B. A. Remington, J. D. Salmonson, and J. L. Kline, Phys. Rev. Lett. **112**, 055002 (2014).

[51] D. S. Clark, J. L. Milovich, D. E. Hinkel *et al.*, Phys. Plasmas **21**, 112705 (2014).